minerals

MDPI

Article

Recrystallization and Uptake of ^{226}Ra into Ba-Rich (Ba,Sr)SO_4 Solid Solutions

Felix Brandt *, Martina Klinkenberg, Jenna Poonoosamy and Dirk Bosbach

Institute of Energy and Climate Research (IEK-6)-Nuclear Waste Management and Reactor Safety, Forschungszentrum Jülich GmbH, 52425 Jülich, Germany; m.klinkenberg@fz-juelich.de (M.K.); j.poonoosamy@fz-juelich.de (J.P.); d.bosbach@fz-juelich.de (D.B.)

* Correspondence: f.brandt@fz-juelich.de; Tel.: +49-2461-61-4205

Received: 24 August 2020; Accepted: 12 September 2020; Published: 15 September 2020

Abstract: ^{226}Ra is an important contributor to naturally occurring radioactive materials (NORM) and also considered in safety cases related to the disposal of spent nuclear fuel in a deep geological repository. Recrystallization and solid solution formation with sulfates is regarded as an important retention mechanism for ^{226}Ra. In natural systems sulfates often occur as (Ba,Sr)SO_4. Therefore, we have chosen this solid solution at the Ba-rich end for investigations of the ^{226}Ra uptake. The resulting ^{226}Ra-solubility in aqueous solution was assessed in comparison with a thermodynamic model of the solid solution-aqueous solution system (Ba,Sr,Ra)SO_4 + H_2O. The temperature and composition of the initial (Ba,Sr)SO_4 solid solution were varied. Measurements of the solution composition were combined with microscopic observations of the solid and thermodynamic modeling. A complex recrystallization behavior of the solid was observed, including the dissolution of significant amounts of the solid and formation of metastable phases. The re-equilibration of Ba-rich (Ba,Sr)SO_4 to (Ba,Sr,Ra)SO_4 leads to a major reconstruction of the solid. Already trace amounts of Sr in the solid solution can have a significant impact on the ^{226}Ra solubility, depending on the temperature. The experimental findings confirm the thermodynamic model, although not all solids reached equilibrium with respect to all cations.

Keywords: radium uptake; recrystallization; (Ba,Sr,Ra)SO_4 solid solution; barite; celestine; nuclear waste management; ternary solid solutions

1. Introduction

The fate of ^{226}Ra is relevant to a number of environmental questions, mainly due to the fact that it is one of the main contributors to naturally occurring radioactive materials (NORM). ^{226}Ra containing NORM appears in many raw material production processes e.g., phosphate industry, unconventional gas production, geothermal energy production, and oil extraction [1–6]. ^{226}Ra is also considered as a relevant radionuclide in safety cases that are prepared for the deep geological disposal of high-level nuclear waste [7–9]. There, it will occur as a fission product of the ^{238}U decay chain and may dominate the dose after about 100,000 years.

The migration of radionuclides in the geosphere is, to a large extent, controlled by sorption processes onto minerals and colloids. On a molecular level, sorption phenomena involve surface complexation, ion exchange as well as co-precipitation reactions. Co-precipitation can lead to the formation of solid solutions in which the radionuclides are structurally incorporated in a host structure [6,8,10]. Such solid solutions are ubiquitous in natural systems—most minerals in nature are mixtures of elements on the molecular scale rather than pure compounds. Recent studies [11–18] have shown that the formation of a (Ba,Ra)SO_4 solid solution significantly reduces the solubility of ^{226}Ra in aqueous systems. Rapid uptake via co-precipitation [11–13] as well as the slower recrystallization

process can lead to this solid solution [14–18]. Recrystallization of $BaSO_4$ in the presence of ^{226}Ra has been considered to be relevant with respect to nuclear waste disposal [19] as well as to ore processing [20,21], where barite was also observed to take up ^{226}Ra from the process solutions.

In order to predict the resulting solubility of ^{226}Ra in such a system, Vinograd et al., 2013 [22] combined theoretical approaches and experimental data. They derived a thermodynamic model for the solid solution-aqueous solution (SS-AS) system $(Ba,Ra)SO_4 + H_2O$ [22]. In natural systems sulfates often occur as $(Ba,Sr)SO_4$ rather than pure barite. Hence, this thermodynamic model was later on extended to the ternary SS-AS system $(Ba,Sr,Ra)SO_4 + H_2O$, and experimentally confirmed for the Sr-rich corner [23–25].

However, the most interesting feature of the predicted system behavior, a minimum of the ^{226}Ra solubility in the Ba-rich corner of the SS-AS system (mole fraction of $SrSO_4$, $X_{SrSO4} < 10$ mol%) still remained experimentally unconfirmed. Here, we have carried out extended long-term recrystallization experiments of more than 660 days in the Ba-rich region of the SS-AS $(Ba,Sr,Ra)SO_4 + H_2O$ and assessed the ^{226}Ra-uptake into the solid as well as the resulting ^{226}Ra-solubility. Macroscopic observations of the solution composition and thermodynamic considerations were combined with microscopic observations to follow in detail the process of solid solution formation due to recrystallization of Ba-rich $(Ba,Sr)SO_4$ put into contact with ^{226}Ra as a function of temperature and initial solid solution composition.

2. Materials and Methods

Homogeneous $(Ba,Sr)SO_4$ solid solutions of a defined composition were synthesized according to the flux method already applied in Klinkenberg et al. (2018) [25]. This method was adapted from procedures of Patel and Koshy (1968) and Patel & Bhat (1971) [26,27]. A detailed characterization of the chemical and morphological homogeneity was carried out by scanning electron microscopy combined with energy-dispersive X-ray spectrometry (SEM-EDX) (Quanta 200F, FEI, Eindhoven, Netherlands; EDAX, Weiterstadt, Germany). The synthesized solids are summarized in Table 1.

Table 1. Overview of synthesized Ba-rich $(Ba,Sr)SO_4$ solid solutions.

Solid Solution	X_{BaSO4}	X_{SrSO4}
$(Ba_{0.95}Sr_{0.05})SO_4$	0.95	0.05 ± 20%
$(Ba_{0.83}Sr_{0.17})SO_4$	0.83	0.17 ± 20%
$(Ba_{0.71}Sr_{0.29})SO_4$	0.71	0.29 ± 20%

The grain size was adjusted to 20–63 µm by grinding and sieving. The chemical homogeneity and morphology of the initial solid solution particles is shown in the back-scatter electron (BSE) image of Figure 1. In order to allow for comparison, the preparation of the solids as well as the general set-up of the recrystallization experiments were adopted from earlier studies (e.g., [17,25]). 0.01 or 0.1 g of solid were added to 10 mL of a 0.2 mol/kg NaCl solution in 25 mL glass vessels. The particles were pre-equilibrated for four weeks at 23 ± 2 °C before the start of the actual experiments to avoid high energy surface sites and ultrafine particles.

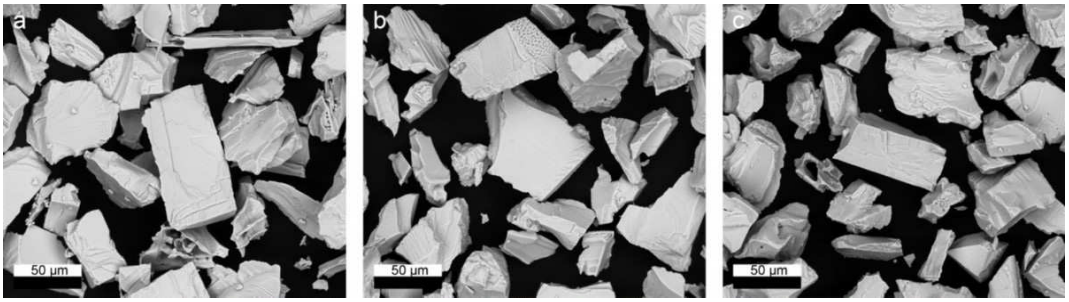

Figure 1. Scanning electron microscope (SEM) images of initial Ba-rich $(Ba,Sr)SO_4$ solid solution particles used for recrystallization experiments. (**a**) $(Ba_{0.95}Sr_{0.05})SO_4$; (**b**) $(Ba_{0.83}Sr_{0.17})SO_4$; (**c**) $(Ba_{0.71}Sr_{0.29})SO_4$.

Long-term batch recrystallization experiments running 664 days were performed at 90 °C, 70 °C and ambient conditions (23 ± 2 °C). 10 mL of tracer solution were added to 10 mL of the pre-equilibrated suspension, resulting in solid/liquid ratios (S/L) of 0.5 g/kg and 5.0 g/kg, respectively, and an ionic strength I = 0.1 mol/kg NaCl. For the same type of glass vessels, in earlier experiments no measurable wall adsorption of ^{226}Ra was detected. All recrystallization experiments were started from a concentration of c(Ra) = 5.5 ± 0.5 × 10^{-6} mol/kg $^{226}RaBr_2$. A summary of the experiments is provided in Table 2.

Table 2. Overview of the recrystallization experiments with Ba-rich (Ba,Sr)SO_4 solid solutions.

Name	Solid/Liquid	c(Ra)	Temperature
	(g/kg)	(10^{-6} mol/kg)	(°C)
$(Ba_{0.95}Sr_{0.05})SO_4$_0.5 g/kg_RT	0.5	5	23 ± 2
$(Ba_{0.83}Sr_{0.17})SO_4$_0.5 g/kg_RT	0.5	5	23 ± 2
$(Ba_{0.71}Sr_{0.29})SO_4$_0.5 g/kg_RT	0.5	5	23 ± 2
Reference $(Ba_{0.95}Sr_{0.05})SO_4$_0.5 g/kg_RT	0.5	0	23 ± 2
Reference $(Ba_{0.83}Sr_{0.17})SO_4$_0.5 g/kg_RT	0.5	0	23 ± 2
Reference $(Ba_{0.71}Sr_{0.29})SO_4$_0.5 g/kg_RT	0.5	0	23 ± 2
$(Ba_{0.95}Sr_{0.05})SO_4$_0.5 g/kg_70	0.5	5	70
$(Ba_{0.83}Sr_{0.17})SO_4$_0.5 g/kg_70	0.5	5	70
$(Ba_{0.71}Sr_{0.29})SO_4$_0.5 g/kg_70	0.5	5	70
Reference $(Ba_{0.95}Sr_{0.05})SO_4$_0.5 g/kg_70	0.5	0	70
Reference $(Ba_{0.83}Sr_{0.17})SO_4$_0.5 g/kg_70	0.5	0	70
Reference $(Ba_{0.71}Sr_{0.29})SO_4$_0.5 g/L_70	0.5	0	70
$(Ba_{0.95}Sr_{0.05})SO_4$_0.5 g/kg_90	0.5	5	90
$(Ba_{0.83}Sr_{0.17})SO_4$_0.5 g/kg_90	0.5	5	90
$(Ba_{0.71}Sr_{0.29})SO_4$_0.5 g/kg_90	0.5	5	90
Reference $(Ba_{0.95}Sr_{0.05})SO_4$_0.5 g/kg_90	0.5	0	90
Reference $(Ba_{0.83}Sr_{0.17})SO_4$_0.5 g/kg_90	0.5	0	90
Reference $(Ba_{0.71}Sr_{0.29})SO_4$_0.5 g/kg_90	0.5	0	90
$(Ba_{0.95}Sr_{0.05})SO_4$_5 g/kg_90	5.0	5	90
$(Ba_{0.83}Sr_{0.17})SO_4$_5 g/kg_90	5.0	5	90
$(Ba_{0.71}Sr_{0.29})SO_4$_5 g/kg_90	5.0	5	90
Reference $(Ba_{0.95}Sr_{0.05})SO_4$_5 g/kg_90	5.0	0	90
Reference $(Ba_{0.83}Sr_{0.17})SO_4$_5 g/kg_90	5.0	0	90
Reference $(Ba_{0.71}Sr_{0.29})SO_4$_5 g/kg_90	5.0	0	90

After a settling time of 1 h, samples of 500 µL of the aqueous solution were taken at the same time intervals for all experiments. The settling time was required for cooling and handling of the radioactive solutions at 70 °C and 90 °C. Based on the experience of Klinkenberg et al., 2018 [25], this is a much shorter time than required for barite and ^{226}Ra to re-equilibrate to the lower temperature. The solution samples were filtered through Advantec ultrafilters (Molecular weight cut-off (MWCO) = 10,000 Da) to avoid possible colloids or fine particles without measurable adsorption of ^{226}Ra at the given filtered solution amount. This procedure was tested in earlier studies [14,15]. Parallel recrystallization experiments without ^{226}Ra were carried out as reference.

A N_2 cooled high-purity (HP) Ge-detector was used for the quantification of the ^{226}Ra concentration at the characteristic 186 keV γ- peak of ^{226}Ra. The Sr and Ba concentrations in solution were quantified using an ICP-MS ELAN 6100 DRC (PerkinElmer SCIEX, Waltham, MA, USA) instrument. The filtered solution was diluted in 0.1 m HNO_3 by 1:1000 for Ba and 1:10,000 for Sr-measurements.

Small amounts of solid (10 µL of the suspension) were sampled at selected sampling times from the settled particles of the recrystallization experiments. The evolution of the crystal morphology and chemical composition were studied using SEM combined with EDX. In order to avoid artefacts due to precipitation of e.g., NaCl, $SrSO_4$ or $RaSO_4$, the samples were separated from their solution by two washing steps in iso-propanol. The samples were then prepared as a suspension on a Cu holder and subsequently dried.

Thermodynamic calculations were carried out to compare theoretical predictions based on a thermodynamic model for the SS-AS system (Ba,Sr,Ra)SO_4 + H_2O with the experimental results. The thermodynamic model derived in Vinograd et al. (2018) [23] and refined in Klinkenberg (2019) [25] was used for the calculation of the total equilibrium between the solid and aqueous phase.

In the case of SS-AS systems, not only do the activities of ions in solution but also of the components of the solid need to be considered. In contrast to pure phases, in SS-AS systems the solution composition is not independent of the amount of solid. For SS-AS equilibria, the solution composition is also linked to the composition of the solid. Gibbs energy minimization approaches implemented in the GEMS3K solver (http://gems.web.psi.ch/GEMS3K) and described in Kulik et al. (2013) [28] were applied to calculate the solid solution composition as well as the aqueous solution equilibria at 23 °C, 70 °C and 90 °C. The equilibria were calculated assuming full equilibration of all (Ba,Sr)SO_4 with ^{226}Ra in solution. The activity coefficients for all dissolved species (γ_j) were calculated according to the extended Debye–Hückel equation [29]. Thermodynamic data for aqueous species were taken from the PSI-Nagra database [30] integrated in GEMS that inherits temperature and pressure dependencies for most aqueous ions and complexes from the Helgeson-Kirkham-flowers equation of state (HKF EoS) [29] as given in the SUPCRT92 database (http://gems.web.psi.ch/TDB). Interaction parameters for the ternary (Ba,Sr,Ra)SO_4 + H_2O SS-AS system were taken from Klinkenberg et al. (2018) [25].

3. Results

3.1. The Evolution of the ^{226}Ra Concentration over Time

Distinct differences with respect to the evolution of the ^{226}Ra concentrations in solution were observed, depending on the composition of the original solid solution (Figure 2). Qualitatively, all experiments follow the trend predicted by the thermodynamic modelling, i.e., the highest uptake of ^{226}Ra is observed at X_{SrSO4} = 29 mol% in the initial solid solution. The kinetics of the ^{226}Ra uptake also follow a trend according to X_{SrSO4} of the initial solid solution, with a slower uptake at low initial X_{SrSO4} and an increasing uptake rate from 17 mol% to 29 mol%.

In particular, the combination of low temperature (23 °C) and a low initial X_{SrSO4} keeps the ^{226}Ra concentration in solution almost on the original level for more than 100 days. Compared to pure $BaSO_4$, the ^{226}Ra uptake is slightly slower in the case of X_{SrSO4} = 5 mol% and faster at higher X_{SrSO4} of the original solid solution (Figure 2). At 70 °C and 90 °C, the ^{226}Ra concentration in solution has a minimum below the predicted equilibrium concentration before equilibrium is approached at later stages of the experiment. This is likely to be a kinetic effect which leads to the metastable "entrapment" of a surplus of ^{226}Ra due to a relatively high uptake rate. This effect was also observed with ^{226}Ra uptake into pure barite in earlier studies [31]. In addition to temperature, the S/L has an effect on the uptake kinetics, resulting in higher ^{226}Ra uptake rate at 90 °C and S/L = 5 g/kg (Figure 3) in comparison to 0.5 g/kg.

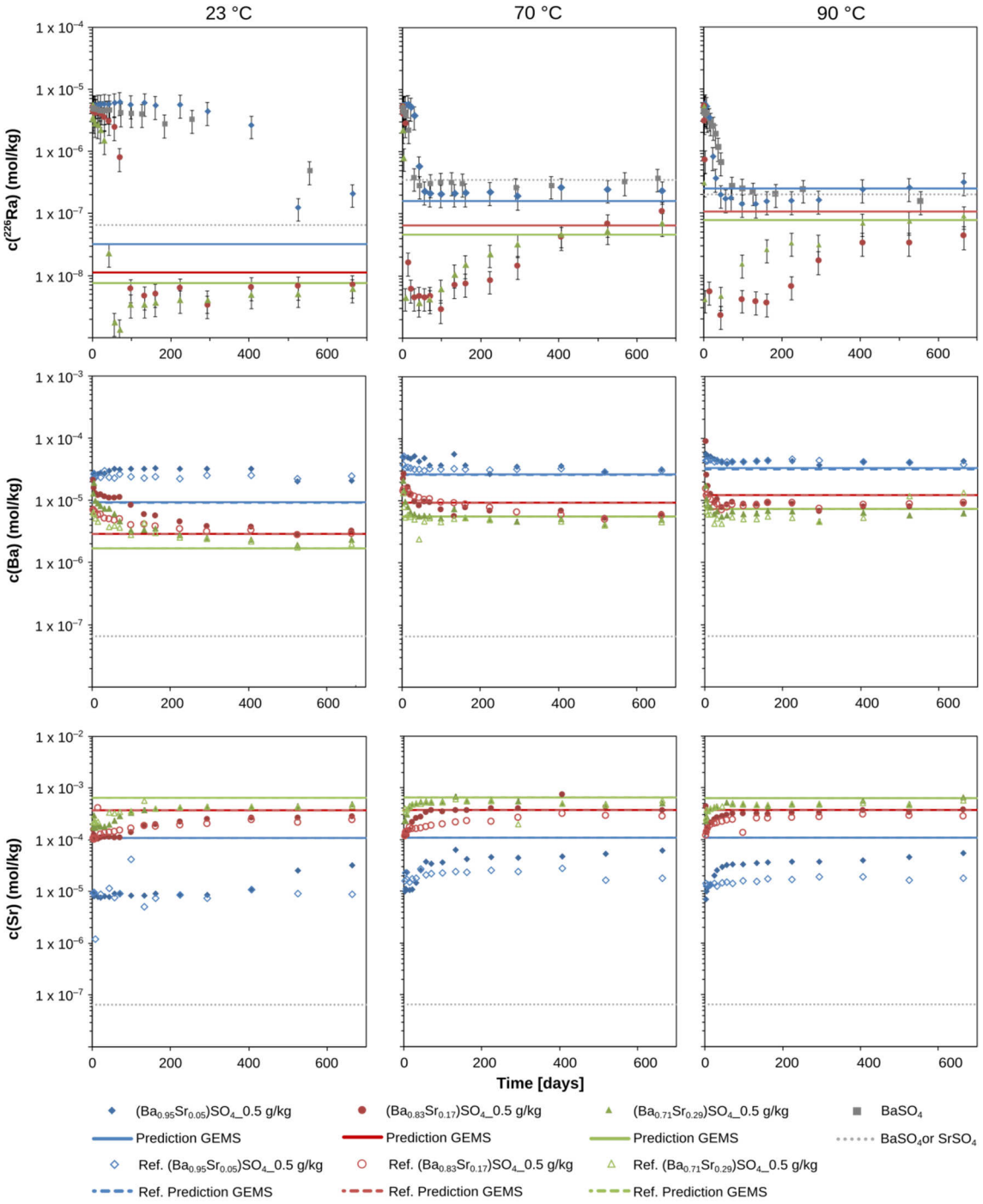

Figure 2. Temporal evolution of the ^{226}Ra, Ba and Sr concentrations in solution for experiments with 0.5 g/kg. Data for pure $BaSO_4$ recrystallization with ^{226}Ra (grey symbols) are taken from experiments with identical solid/liquid ratios, ionic strength and temperature as published in [24,31]. The grey dotted line in the c(Sr) vs. time plot refer to the solubility of pure $SrSO_4$, and to pure $BaSO_4$ in the other two plots. Data are given in the Appendix A Tables A1–A20. The thermodynamic predictions (lines) are based on [23,25].

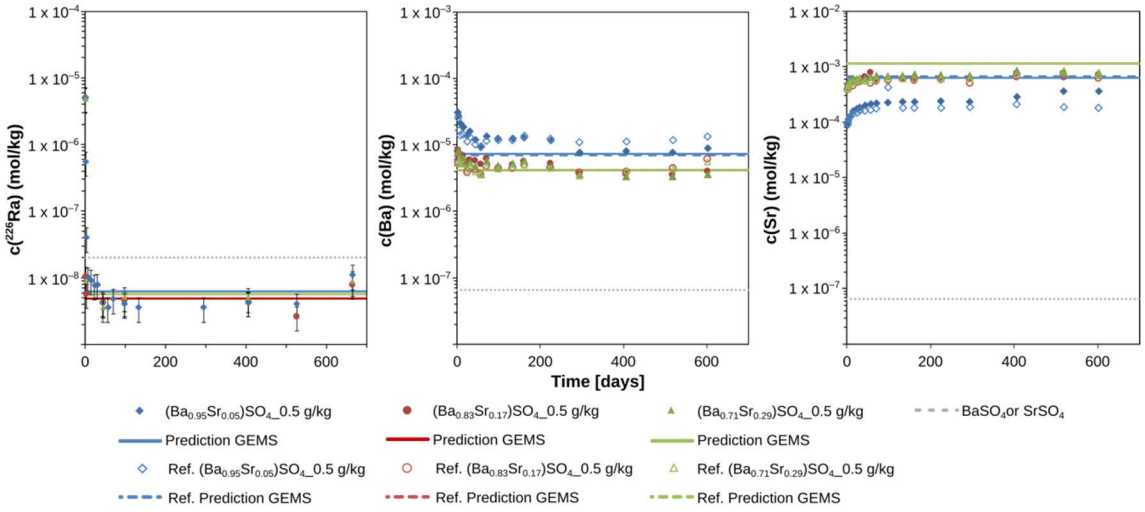

Figure 3. Temporal evolution of the ^{226}Ra, Ba and Sr concentrations in solution for experiments with 5 g/kg and 90 °C. Data are given in the Appendix A Tables A1–A20. The thermodynamic predictions (lines) are based on [23,25].

Within 100 days, the majority of the recrystallization experiments reach a plateau of the ^{226}Ra concentrations which is close to the predicted equilibrium (lines in Figure 2). At 23 °C and S/L = 0.5 g/kg, the effect of Sr added to the SS-AS system results in a significant decrease of the Ra solubility. Compared to pure $BaSO_4$ this decrease can be up to one order of magnitude. The predicted ^{226}Ra-solubilities for the respective experiments become more similar with increasing temperatures of 70 °C and 90 °C. This is also experimentally observed for the final ^{226}Ra concentrations in this study. At 90 °C, the observed and predicted differences of the ^{226}Ra solubility between the different solid solutions and pure $BaSO_4$ are small and within the experimental error (Figure 2). At 90 °C and S/L = 5 g/kg, the predicted results of the ^{226}Ra solubility as well as the experimental results are almost independent from the original X_{SrSO4} of the solid solution (Figure 3).

3.2. The Evolution of Ba and Sr Concentrations over Time

As shown in Figure 2, the presence of ^{226}Ra has a rather small impact on the calculated equilibrium concentrations of Ba and Sr in solution. The predicted Ba-solubility at all temperatures decreases in the order from Ba-rich to Ba-poor original solid solutions whereas the Sr-solubility increases from Sr-rich to Sr-poor original solid solutions. Therefore, the final predicted solids are much more similar to each other in composition than the original solid solutions before re-equilibration (Table 3). Due to the high proportion of total (Ba + Sr) compared to the amount of ^{226}Ra added to the respective experiment, the predictions for the Ba and Sr solubility after recrystallization are very similar for corresponding ^{226}Ra-free reference experiments and the ^{226}Ra-recystallization experiments.

A comparison of the experimental results and predicted equilibrium indicates Ba to be supersaturated in the aqueous solution at the beginning of all experiments. The concentration of Sr in solution starts from values well below the predicted equilibrium and usually approaches equilibrium later than Ba. After 200 to 400 days, in most of the experiments the concentrations of Sr and Ba are close to or at the predicted equilibrium (Figure 2). The kinetic behavior of the (Ba,Sr)SO_4 recrystallization is more or less independent of the presence of ^{226}Ra. In the series of ^{226}Ra free reference experiments, the experiment with X_{SrO4} = 5 mol% is an exception because the concentration of Sr in solution in particular stays well below the predicted equilibrium, and at 23 °C the Ba concentration stays higher than predicted-similar to the corresponding ^{226}Ra recrystallization experiment.

Table 3. Calculated equilibrium compositions of solid solutions after total equilibration of the system (X for mole fraction).

Experiment	Composition of Solid Solution Present at Equilibrium		
	X_{BaSO4}	X_{RaSO4} (%)	X_{SrSO4}
$(Ba_{0.95}Sr_{0.05})SO_4$_0.5 g/kg_RT	99.74	0.24	0.02
$(Ba_{0.83}Sr_{0.17})SO_4$_0.5 g/kg_RT	99.52	0.27	0.21
$(Ba_{0.71}Sr_{0.29})SO_4$_0.5 g/kg_RT	99.06	0.31	0.63
Reference $(Ba_{0.95}Sr_{0.05})SO_4$_0.5 g/kg_RT	99.99	-	0.01
Reference $(Ba_{0.83}Sr_{0.17})SO_4$_0.5 g/kg_RT	99.83	-	0.17
Reference $(Ba_{0.71}Sr_{0.29})SO_4$_0.5 g/kg_RT	99.49	-	0.51
$(Ba_{0.95}Sr_{0.05})SO_4$_0.5 g/kg_70	99.72	0.24	0.04
$(Ba_{0.83}Sr_{0.17})SO_4$_0.5 g/kg_70	99.29	0.27	0.44
$(Ba_{0.71}Sr_{0.29})SO_4$_0.5 g/kg_70	98.34	0.30	1.36
Reference $(Ba_{0.95}Sr_{0.05})SO_4$_0.5 g/kg_70	99.96	-	0.04
Reference $(Ba_{0.83}Sr_{0.17})SO_4$_0.5 g/kg_70	99.63	-	0.37
Reference $(Ba_{0.71}Sr_{0.29})SO_4$_0.5 g/L_70	98.88	-	1.12
$(Ba_{0.95}Sr_{0.05})SO_4$_0.5 g/kg_90	99.69	0.23	0.07
$(Ba_{0.83}Sr_{0.17})SO_4$_0.5 g/kg_90	99.17	0.26	0.57
$(Ba_{0.71}Sr_{0.29})SO_4$_0.5 g/kg_90	97.60	0.30	2.10
Reference $(Ba_{0.95}Sr_{0.05})SO_4$_0.5 g/kg_90	99.94	-	0.06
Reference $(Ba_{0.83}Sr_{0.17})SO_4$_0.5 g/kg_90	99.42	-	0.58
Reference $(Ba_{0.71}Sr_{0.29})SO_4$_0.5 g/kg_90	98.24	-	1.76
$(Ba_{0.95}Sr_{0.05})SO_4$_5 g/kg_90	97.83	0.02	2.15
$(Ba_{0.83}Sr_{0.17})SO_4$_5 g/kg_90	90.21	0.02	9.77
$(Ba_{0.71}Sr_{0.29})SO_4$_5 g/kg_90	90.20	0.03	9.77
Reference $(Ba_{0.95}Sr_{0.05})SO_4$_5 g/kg_90	98.02	-	1.98
Reference $(Ba_{0.83}Sr_{0.17})SO_4$_5 g/kg_90	92.55	-	7.45
Reference $(Ba_{0.71}Sr_{0.29})SO_4$_5 g/kg_90	92.55	-	7.45

3.3. Chemical and Microstructural Evolution of the Solid

The solid composition corresponding to the respective aqueous solution of each experiment at a given time is accessible in two independent ways, (1) via mass balance between original solid composition and solution at a given time and (2) via microchemical (SEM-EDX) analyses of individual particles. While (1) indicates the general evolution of the system, (2) can be used to evaluate the variation of particle morphology, composition and homogeneity during the approach to equilibrium. Based on the results in 3.2, three extreme examples are discussed here:

(1) X_{SrSO4} = 5 mol%, 23 °C, S/L = 0.5 g/kg, slow macroscopic recrystallization kinetics;

(2) X_{SrSO4} = 29 mol%, 23 °C, S/L = 0.5 g/kg, fast macroscopic recrystallization kinetics and ^{226}Ra entrapment;

(3) X_{SrSO4} = 5 mol%, 90 °C, 5 g/kg, fast macroscopic recrystallization kinetics, no entrapment of ^{226}Ra.

The evolution of the average particle composition (mass balance) versus the ^{226}Ra concentration in solution for the three examples is depicted in Figure 4. Starting at the initial ^{226}Ra concentration of ca. 5.5×10^{-6} mol/kg (broken line in Figure 4), ^{226}Ra in solution drops up to three orders of magnitude while X_{SrSO4} stays more or less constant. At 23 °C, the calculated average X_{SrSO4} stays constant for the $(Ba_{0.95}Sr_{0.05})SO_4$ solid solution during the complete experiment, and more than 42 days for $(Ba_{0.71}Sr_{0.29})SO_4$ (arrows in Figure 4a). In the recrystallization experiment with 5 g/kg $(Ba_{0.95}Sr_{0.05})SO_4$ and 90 °C, already after 42 days the concentration of ^{226}Ra in solution is close to the final value. The average X_{SrSO4} only changes from 5 mol% to 4.1 mol% after 42 days. Only minor adjustments of the ^{226}Ra and Sr concentrations in solution are observed later on (Figure 4b).

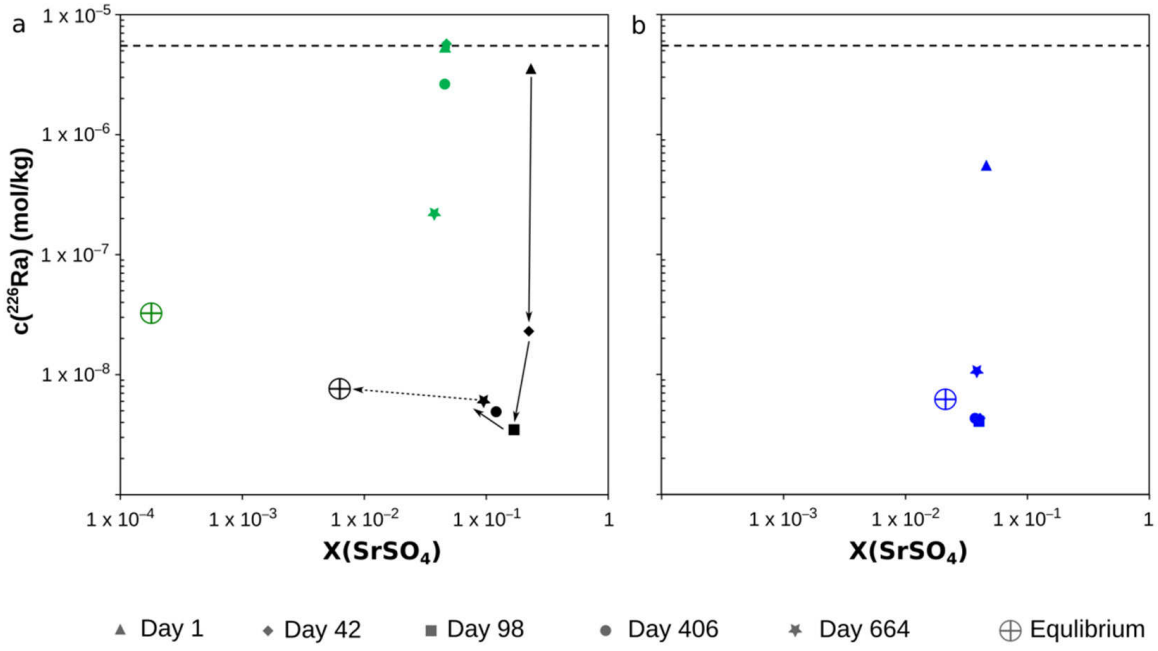

Figure 4. Temporal evolution of the ^{226}Ra concentration in solution and the average mole fraction X_{SrSO4} of the corresponding solid during the recrystallization experiments; (**a**) green symbols are X_{SrSO4} = 5 mol%, 23 °C, 0.5 g/kg, black symbols are X_{SrSO4} = 29 mol%, 23 °C, 0.5 g/kg, (**b**) blue symbols are X_{SrSO4} = 5 mol%, 90 °C, 5 g/kg; the corresponding predicted equilibria are symbolized by the crosshairs in the respective color. The black dashed line indicates the initial ^{226}Ra concentration.

For the solids of this study, mainly Sr and Ba can be quantified by EDX whereas ^{226}Ra can only be quantified with this method at local concentrations of more than 0.5 at%. Depending on the chemical and morphological variability, between 5 and 25 EDX spot measurements were carried out on each powder sample. The best match between the average compositions obtained via EDX and mass balance for a given sampling time were observed at the end of the experiments. Here, the average X_{SrSO4} and X_{BaSO4} obtained by both methods agree within experimental error (Table 4). However, the X_{SrSO4} still deviates significantly from the calculated equilibrium. A trend in the temporal evolution towards the equilibrium composition is visible in Table 4 and Figure 4 and discussed in more detail in Section 4.

The X_{SrSO4} of individual particles as well as their morphology were analyzed as a function of time. For experiment $(Ba_{0.95}Sr_{0.05})SO_4$_0.5 g/kg_RT, during the first 98 days the grain morphology remained almost unchanged. Steps on the surface due to cleavage during sample preparation were still visible at day 98 (Figure 5). The chemical composition of the particles at a given sampling time in this series was quite variable until the end of this experiment, with a range of X_{SrSO4} between 0.4 and 9.8 mol% (Table A21).

The morphology of the particles taken from experiment $(Ba_{0.71}Sr_{0.29})SO_4$_0.5 g/kg_RT changed after day 1 as large cavities occurred. At day 42 and 98, new smooth surfaces were visible in some areas whereas the cavities appeared to become smaller (Figure 5). Coatings were typical on some surfaces whereas other surfaces were interrupted by cavities. Some particles still contained almost 2/3 of the original $SrSO_4$. The early morphological evolution over time of the particles taken from experiment $(Ba_{0.71}Sr_{0.29})SO_4$_5 g/kg_90 was similar to $(Ba_{0.71}Sr_{0.29})SO_4$_0.5 g/kg_RT, just faster. The grains lost their cavities and developed smooth, well defined surfaces with time. Simultaneously to the morphological evolution, the X_{SrSO4} shifted towards lower values. However, even at the end of the experiments, the particles were not homogeneous but Sr-rich and Sr-poor zones in individual particles were observed (Figure 5, spots 4 and 5).

Table 4. Average solid compositions (X = mole fractions) after day 1, 42, 98 and 664 compared to calculated composition from solution and equilibrium composition calculated by GEMS. All measured energy-dispersive X-ray spectrometry (EDX) data are given in the Appendix A in Tables A21–A23.

Day	Method	Number of Particles EDS-Analyses		X_{SrSO4} Minimum (%)	X_{SrSO4} Maximum (%)	X_{SrSO4} Average (%)
		$(Ba_{0.95}Sr_{0.05})SO_4$_0.5 g/kg_RT				
1	EDX	5	5	3.5	9.8	6.2
	Mass balance					4.6
42	EDX	5	7	2.9	8.2	5.0
	Mass balance					4.7
98	EDX	5	7	3.2	10.3	5.8
	Mass balance					4.7
664	EDX	9	21	0.4	9.8	4.1
	Mass balance					3.6
	Calculated equilibrium					**0.3**
		$(Ba_{0.71}Sr_{0.29})SO_4$_0.5 g/kg_RT				
1	EDX	6	12	4.3	30.5	17.0
	Mass balance					23.2
42	EDX	5	9	5.4	27.9	13.4
	Mass balance					22.3
98	EDX	6	11	6.9	24.3	14.1
	Mass balance					16.9
664	EDX	10	25	4.7	21.4	9.9
	Mass balance					9.5
	Calculated equilibrium					**0.6**
		$(Ba_{0.95}Sr_{0.05})SO_4$_5 g/kg_90				
1	EDX	4	7	3.9	13.6	8.5
	Mass balance					4.6
42	EDX	4	5	1	4.1	2.5
	Mass balance					4.1
98	EDX	6	6	0.8	7	3.0
	Mass balance					4.0
664	EDX	9	14	1.6	6.3	3.9
	Mass balance					3.4
	Calculated equilibrium					**2.2**

In addition to the differences in the morphological evolution with time, also the chemical homogeneity and local enrichment of ^{226}Ra varied among the experimental series. The ^{226}Ra uptake for experiment $(Ba_{0.95}Sr_{0.05})SO_4$_0.5 g/kg_RT was mainly homogenous—only a small number of EDX spectra detected an enrichment of ^{226}Ra. Only at the end of this experiment, some areas showed a significant ^{226}Ra enrichment (spot 1 of Figure 5, Table A21). ^{226}Ra-rich areas were detected on some particles, often small particles associated with the surfaces of larger particles. At higher X_{SrSO4} and 23 °C, already at the beginning ^{226}Ra-rich areas in some particles were observed (Table A22; spot 2 in Figure 5). The surfaces appeared to be covered by Ba–Ra-rich coatings (spot 3 in Figure 5). In experiment $(Ba_{0.71}Sr_{0.29})SO_4$_5 g/kg_90, between day 1 and day 98 ^{226}Ra was detected in significant amounts in the solid phase, usually associated with higher X_{BaSO4} as well. A complete homogenization of the solid was not observed in any experiment.

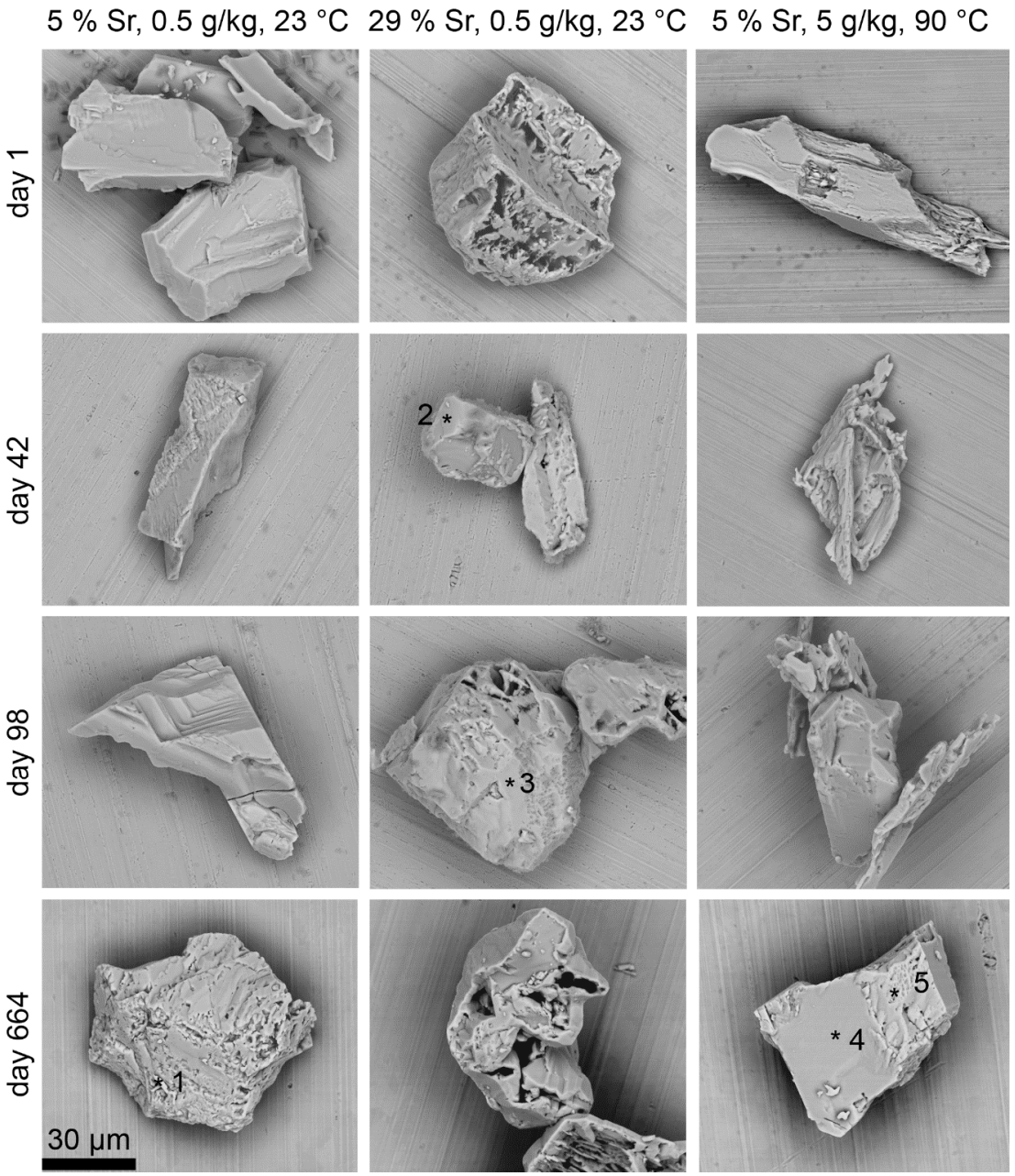

Figure 5. SEM micrographs of representative particles taken from recrystallization experiments with X_{SrSO4} = 5 mol%, 23 °C, 0.5 g/kg, X_{SrSO4} = 29 mol%, 23 °C, 0.5 g/kg, and X_{SrSO4} = 5 mol%, 90 °C, 5 g/kg. The numbered spots marked with (*1, *2, *3, *4, *5) represent the areas where EDX analyses were taken (Tables A21–A23).

4. Discussion

4.1. Effect of X_{SrSO4} upon the Solubility of ^{226}Ra

The theoretically derived thermodynamic model for the SS-AS system (Ba,Sr,Ra)SO_4 of Vinograd et al. (2018) [23] predicts a significant impact of the mole fraction X_{SrSO4} upon the solubility of ^{226}Ra. Depending on temperature, the ^{226}Ra solubility is expected to vary up to several orders of magnitude in the range of X_{SrSO4} between 0 and 10 mol%. According to the model, the re-equilibration of Ba-rich (Ba,Sr)SO_4 to (Ba,Sr,Ra)SO_4 requires a major reconstruction of the solid. In order to reach equilibrium, a large fraction of more than 95 mol% of the Sr formerly present in the solid needs to be released

into the aqueous solution while ^{226}Ra is taken up. At the same time they indicate that already trace amounts of Sr in the solid solution can have a significant impact on the ^{226}Ra solubility if the solid solution is in full equilibrium with the aqueous solution. According to these calculations, this impact depends on temperature as well, i.e., at 23 °C the differences between the ^{226}Ra solubilities are more pronounced than at 70 °C or 90 °C.

On the macroscopic side, the experimental findings are coherent with the thermodynamic model. In particular, the plateau of the final c(^{226}Ra) in solution was close to the predicted equilibrium. The final Ba and Sr concentrations in solution approached equilibrium, but especially Sr in solution deviated significantly from the prediction in some of the experiments, indicating that these were still not at equilibrium (Figure 6). Within the duration of the experiments at 23 °C, X_{SrSO4} was not completely adjusted to equilibrium in any solid. In particular, the experiments with only 5 mol% $SrSO_4$ in the initial solid solution didn't reach equilibrium, but at high temperature and high S/L the deviation for the same initial solid solution composition became small, close to the experimental error (Figure 6b).

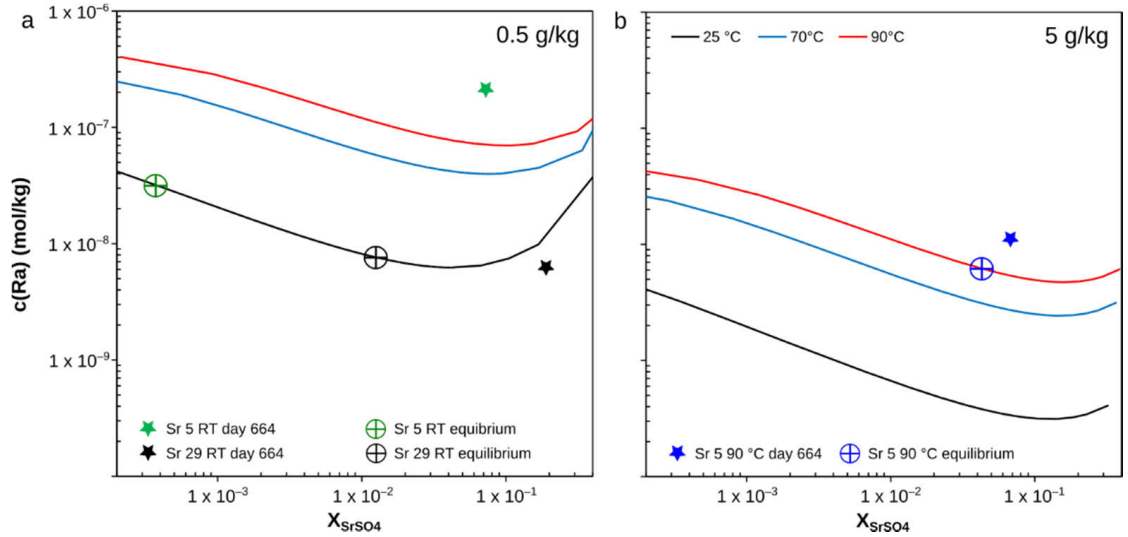

Figure 6. Calculated ^{226}Ra solubility curves as a function of X_{SrSO4} in the solid solution in equilibrium with the aqueous solution. Experimental end points (stars) are compared with theoretical equilibria (crosshairs). (**a**) experiments with a solid/liquid ratio of 0.5 g/kg; (**b**) 5 g/kg.

4.2. Kinetics of the Recrystallization from (Ba,Sr)SO_4 to (Ba,Sr,Ra)SO_4

The SS-AS system is dominated by the re-equilibration of (Ba,Sr)SO_4. All three original (Ba,Sr)SO_4 solid solutions need to release only a very low proportion of total $BaSO_4$ from the solid to reach the predicted equilibrium solution composition, i.e., dissolution at the surface is sufficient to fulfill this condition. On the other hand, more than 97 mol% of the $SrSO_4$ originally present in the solid solutions of this study would need to be released from the solid into the aqueous solution in order to reach equilibrium. Taking into account the amount to be released from the solid, $SrSO_4$ may be more accessible to dissolution at the particle surfaces in the case of higher X_{SrSO4}, and therefore equilibrium may be reached earlier.

Brandt et al., 2018 [32] have shown that in certain combinations of S/L and temperature, Sr_{aq} can inhibit the recrystallization of $BaSO_4$ and the uptake of ^{226}Ra. Therefore, at 23 °C and low X_{SrSO4} the system may behave similar to pure $BaSO_4$, and the presence of Sr in solution may thus slow down the kinetics of recrystallization. The solid solution with initially only X_{SrSO4} = 5%, recrystallized at 23 °C, appeared to undergo very little change of X_{SrSO4} with time (Figure 6a). A higher X_{SrSO4} of the original solid solution lead to faster ^{226}Ra uptake kinetics, and in some cases even to a minimum of the ^{226}Ra concentration, which was attributed to a kinetic "entrapment" effect. The faster re-equilibration correlated with the higher solubility of $SrSO_4$ compared to the other two sulfates.

For a given composition, ^{226}Ra appeared to be adjusted more or less independent of Sr. As soon as ^{226}Ra was structurally taken up, the concentration in solution dropped by several orders of magnitude whereas the re-structuring of the solid towards a full equilibrium required several steps of dissolution and re-precipitation as microscopically observed. Microscopically, the recrystallization of the binary (Ba,Sr)SO_4 solid solution to (Ba,Sr,Ra)SO_4 is a complex process that is clearly different from the replacement reaction observed for the formation of (Ba,Ra)SO_4 from barite [31]. Instead, the re-equilibration lead to similar features as observed in earlier studies on the reaction of $SrSO_4$ with Ba in solution [33] and on the recrystallization of Sr-rich (Sr,Ba)SO_4 in the presence of ^{226}Ra [25]. Rims of newly formed phases were observed on the original particles. The original particles dissolved partially, leaving large cavities in the original grains of some experiments presented here. Already, at the beginning of the experiments with high X_{SrSO4} in the original solid solution, or at high temperature and solid/liquid ratio, theses cavities indicate a significant dissolution. Later on, the particles of the experiment with higher X_{SrSO4} changed in their morphology and new smooth surfaces became visible in some areas whereas the cavities appeared to become smaller. In some areas, an idiomorphic habitus occurred. However, even at day 664 the morphology and also X_{SrSO4} were still not at equilibrium (Figure 6). In many cases, the particles remained chemically heterogeneous. Simultaneously to the morphological evolution, the X_{SrSO4} changed, with X_{SrSO4} in some measurements even below the predicted equilibrium. Therefore, the grain morphology apparently followed the macroscopically observed recrystallization kinetics.

At slow recrystallization rates as observed for experiment ($Ba_{0.95}Sr_{0.05}$)SO_4_0.5 g/kg_RT, during the first 98 days the grain morphology remained almost unchanged. Here, the cavities which were observed early on in the other experiments occurred at the end of the experiment.

5. Conclusions

The newly derived thermodynamic model for the SS-AS system (Ba,Sr,Ra)SO_4 + H_2O [23,25] was tested in recrystallization experiments at the Ba-rich corner. In contrast to pure barite, in the ternary system significant dissolution and neo-formation of particles with a more ideal particle morphology occurs. A simultaneous evolution of the grain morphology and the X_{SrSO4} was observed. After 664 days, many experiments reach a partial equilibrium with c(^{226}Ra) already close to the predicted values. Most experiments approach the predicted equilibrium concentrations of Ba and Sr, but only the experiments with high X_{SrSO4} in the original solid reached the predicted equilibrium within the duration of the experiments.

In conclusion, the trends predicted by the thermodynamic model of Vinograd et al. (2018) [23] and a favorable role of small amounts of Sr in the (Ba,Sr)SO_4 solid solution with respect to the uptake of ^{226}Ra can be confirmed by this study.

Author Contributions: Conceptualization, F.B. and M.K.; validation, F.B.; investigation, F.B., M.K. and J.P.; data curation, M.K. and J.P.; writing—original draft preparation, F.B., J.P. and M.K.; writing—review and editing, D.B. and J.P.; visualization, M.K. and J.P.; project administration, F.B.; funding acquisition, F.B. and D.B. All authors have read and agreed to the published version of the manuscript.

Funding: The research leading to these results has received partial funding from the German Federal Ministry of Education and Research (BMBF) ThermAc3 project (project number 02NUK039D).

Acknowledgments: We are grateful to Murat Güngör, Dimitri Schneider, Fabian Kreft, Andreas Wilden, Ralf König and Giuseppe Modolo for their support.

Conflicts of Interest: The authors declare no conflict of interest.

Appendix A

Table A1. ^{226}Ra concentrations in solution of the experiments at 23 °C.

Day	Ra Concentration in Solution (10^{-8} mol/kg)		
	$(Ba_{0.95}Sr_{0.05})SO_4$_0.5 g/kg_RT	$(Ba_{0.83}Sr_{0.17})SO_4$_0.5 g/kg_RT	$(Ba_{0.71}Sr_{0.29})SO_4$_0.5 g/kg_RT
0.5	536	523	559
1	542	442	355
3	551	433	324
7	550	406	280
14	568	431	268
21	569	404	223
30	580	357	148
42	571	302	2.30
56	600	247	0.18
70	625	79.4	0.14
98	556	0.61	0.35
133	605	0.47	0.35
161	544	0.51	0.37
224	568	0.63	0.41
294	438	0.34	0.41
406	264	0.65	0.49
525	12.5	0.68	0.51
664	20.9	0.72	0.61
Equilibrium (GEMS)	3.24	1.13	0.76

Table A2. ^{226}Ra concentrations in solution of the experiments at 70 °C.

Day	Ra Concentration (10^{-8} mol/kg)		
	$(Ba_{0.95}Sr_{0.05})SO_4$_0.5 g/kg_70	$(Ba_{0.83}Sr_{0.17})SO_4$_0.5 g/kg_70	$(Ba_{0.71}Sr_{0.29})SO_4$_0.5 g/kg_70
0.5	546	534	531
1	552	441	222
3	539	402	80.0
7	559	281	0.45
14	576	1.66	
21	519	0.61	
30	378	0.45	
42	58.3	0.47	0.37
56	23.1	0.45	
70	21.5	0.47	
98	20.9	0.29	0.61
133	21.3	0.72	1.06
161	21.7	0.76	1.51
224	22.5	0.85	2.25
294	19.2	1.46	3.27
406	26.4	4.30	4.70
525	24.7	6.95	5.32
664	23.5	0.11	7.16
Equilibrium (GEMS)	16.2	6.55	4.59

Table A3. ^{226}Ra concentrations in solution of the experiments at 90 °C.

Day	Ra Concentration (10^{-8} mol/kg)		
	$(Ba_{0.95}Sr_{0.05})SO_4$_0.5 g/kg_90	**$(Ba_{0.83}Sr_{0.17})SO_4$_0.5 g/kg_90**	**$(Ba_{0.71}Sr_{0.29})SO_4$_0.5 g/kg_90**
0.5	546	541	532
1	547	308	30.5
3	576	72.2	0.41
7	522		
14	344	0.55	
21	80.8		
30	36.2		
42	19.8	0.22	0.45
56	17.0		
70	17.6		
98	14.1	0.41	0.51
133	14.0	0.38	
161	15.7	0.36	2.64
224	15.8	0.67	3.35
294	16.1	1.70	3.11
406	24.2	3.35	6.95
525	25.6	3.35	7.43
664	31.6	4.31	9.10
Equilibrium (GEMS)	24.9	10.6	7.78

Table A4. ^{226}Ra concentrations in solution of the experiments at 90 °C and solid/liquid ratio (S/L) = 5 g/kg.

Day	Ra Concentration (10^{-8} mol/kg)		
	$(Ba_{0.95}Sr_{0.05})SO_4$_5 g/kg_90	**$(Ba_{0.83}Sr_{0.17})SO_4$_5 g/kg_90**	**$(Ba_{0.71}Sr_{0.29})SO_4$_5 g/kg_90**
0.5	507	503	490
1	55.4	1.02	0.86
42	0.43	0.41	0.37
98	0.41	0.45	0.51
406	0.43	0.43	0.51
664	1.10	0.79	0.89
Equilibrium (GEMS)	0.62	0.49	0.57

Table A5. Ba concentrations in solution of the experiments at 23 °C.

Day	Ba Concentration (10^{-6} mol/kg)		
	$(Ba_{0.95}Sr_{0.05})SO_4$_0.5 g/kg_RT	$(Ba_{0.83}Sr_{0.17})SO_4$_0.5 g/kg_RT	$(Ba_{0.71}Sr_{0.29})SO_4$_0.5 g/kg_RT
1		20.9	12.9
3	27.4	15.7	19.1
7	26.6	13.1	9.83
14	26.5	12.2	9.00
21	27.6	12.5	8.21
30	27.1	11.4	7.45
42	30.0	10.9	7.41
56	31.9	11.0	6.06
70	31.1	11.1	4.62
98	32.3	8.40	3.27
133	32.3	5.91	3.35
161	33.1	5.69	3.53
224	32.2	4.51	2.79
294	32.2	3.81	2.52
406	31.9	3.69	2.32
525	20.2	2.79	1.92
664	20.9	3.26	2.35
Equilibrium (GEMS)	9.40	2.90	1.70

Table A6. Ba concentrations in solution of the reference experiments without ^{226}Ra, 23 °C.

Day	Ba Concentration (10^{-6} mol/kg)		
	Reference $(Ba_{0.95}Sr_{0.05})SO_4$_0.5 g/kg_RT	Reference $(Ba_{0.83}Sr_{0.17})SO_4$_0.5 g/kg_RT	Reference $(Ba_{0.71}Sr_{0.29})SO_4$_0.5 g/kg_RT
1	22.7	7.06	6.39
3	26.3	6.70	6.11
7	23.3	6.41	5.10
14	1.82	5.83	4.59
21	23.1	5.90	0.08
30	29.9	5.17	0.17
42	23.6	4.95	3.75
56	22.7	4.81	3.88
70	26.2	4.95	3.60
98	24.2	4.00	2.77
133	22.6	4.08	4.35
161	24.0	3.86	3.02
224	22.4	3.50	2.53
294	25.0	3.13	2.41
406	25.0	3.27	2.18
525	22.4	2.77	1.74
664	24.4	2.92	1.94
Equilibrium (GEMS)	9.05	2.87	1.69

Table A7. Ba concentration of experiments at 70 °C.

Day	Ba Concentration (10^{-6} mol/kg)		
	$(Ba_{0.95}Sr_{0.05})SO_4$_0.5 g/kg_70	$(Ba_{0.83}Sr_{0.17})SO_4$_0.5 g/kg_70	$(Ba_{0.71}Sr_{0.29})SO_4$_0.5 g/kg_70
1	50.0	22.7	21.3
3	49.3	26.7	14.5
7		13.9	9.69
14	50.0	16.4	7.88
21	47.2	12.7	6.53
30	52.0	9.63	6.11
42	42.5	8.37	5.64
56	48.8	9.74	5.85
70	37.3	9.45	5.68
98	37.3	7.19	5.28
133	56.3	5.67	7.41
161	37.5	7.81	5.40
224	27.3	6.90	5.10
294	35.5		4.66
406	36.1	6.83	5.19
525	29.3	5.26	4.26
664	31.7	6.08	4.98
Equilibrium (GEMS)	26.6	9.42	5.62

Table A8. Ba concentrations in solution of the reference experiments without ^{226}Ra, 70 °C.

Day	Ba Concentration (10^{-6} mol/kg)		
	Reference $(Ba_{0.95}Sr_{0.05})SO_4$_0.5 g/kg_70	Reference $(Ba_{0.83}Sr_{0.17})SO_4$_0.5 g/kg_70	Reference $(Ba_{0.71}Sr_{0.29})SO_4$_0.5 g/kg_70
1	38.0	14.3	13.2
3	52.7	15.6	7.88
7	34.0	13.7	5.42
14	34.1	14.6	5.91
21	33.5	12.6	5.57
30	31.7	11.8	5.04
42	32.1	11.3	2.41
56	30.4	10.5	4.66
70	32.8	10.6	5.32
98	32.0	9.54	4.56
133	33.1	9.32	5.08
161	31.8	8.81	5.24
224	31.3	7.72	4.91
294	32.0	6.63	0.85
406	33.1	5.96	4.66
525	29.1	5.03	4.07
664	30.8	5.85	4.52
Equilibrium (GEMS)	2.58	9.29	5.58

Table A9. Ba concentration of experiments at 90 °C.

Day	Ba Concentration (10^{-6} mol/kg)		
	$(Ba_{0.95}Sr_{0.05})SO_4$_0.5 g/kg_90	**$(Ba_{0.83}Sr_{0.17})SO_4$_0.5 g/kg_90**	**$(Ba_{0.71}Sr_{0.29})SO_4$_0.5 g/kg_90**
1	56.2	90.3	17.2
3	51.8	25.8	10.7
7	52.5	16.8	8.60
14	51.2	12.6	7.86
21	46.4	9.17	6.07
30	44.6	10.4	6.74
42	40.7	7.73	5.50
56	38.9	8.52	5.80
70	43.0	9.40	6.69
98	42.2	8.69	6.15
133	43.1	8.74	6.29
161	43.3	8.96	6.79
224	42.9	8.72	6.66
294	36.8	6.73	4.70
406	41.8	7.98	6.40
525	40.4	7.96	5.73
664	42.6	8.72	6.29
Equilibrium (GEMS)	32.9	12.2	7.39

Table A10. Ba concentrations in solution of the reference experiments without ^{226}Ra, 90 °C.

Day	Ba Concentration (10^{-6} mol/kg)		
	Reference $(Ba_{0.95}Sr_{0.05})SO_4$_0.5 g/kg_90	**Reference $(Ba_{0.83}Sr_{0.17})SO_4$_0.5 g/kg_90**	**Reference $(Ba_{0.71}Sr_{0.29})SO_4$_0.5 g/kg_90**
1	43.5	15.6	8.69
3	43.3	12.1	6.74
7	44.1	11.0	5.94
14	45.2	10.4	5.87
21	42.0	7.99	4.23
30	43.1	8.69	5.07
42	41.8	7.09	4.20
56	42.2	7.72	
70	42.0	8.61	5.34
98	42.2	8.26	5.04
133	43.4	8.39	4.98
161	44.1	9.20	5.57
224	46.3	9.11	5.29
294	43.9	7.32	4.51
406	42.1	8.49	5.20
525	40.5	8.76	11.6
664	38.2	9.30	13.2
Equilibrium (GEMS)	32.0	12.1	0.32

Table A11. Ba concentration of experiments at 90 °C and S/L = 5 g/kg.

Day	Ba concentration (10^{-6} mol/kg)		
	$(Ba_{0.95}Sr_{0.05})SO_4$_5 g/kg_90	**$(Ba_{0.83}Sr_{0.17})SO_4$_5 g/kg_90**	**$(Ba_{0.71}Sr_{0.29})SO_4$_5 g/kg_90**
1	30.9	7.81	7.59
3	27.2	8.33	8.32
7	20.7	7.14	6.45
14	18.6	6.81	6.28
21	13.8	5.04	4.70
30	15.8	5.93	5.46
42	12.1	5.72	4.67
56	9.66	5.12	3.60
70	13.6	6.11	5.77
98	12.5	0.00	4.82
133	12.6	4.95	5.15
161	12.6	5.59	5.72
224	11.6	5.19	4.75
294	7.72	3.60	3.63
406	8.15	3.56	3.33
525	7.64	3.51	3.35
664	8.97	3.99	3.60
Equilibrium (GEMS)	7.37	4.16	4.16

Table A12. Ba concentration of the reference experiments without ^{226}Ra at 90 °C and S/L = 5 g/kg.

Day	Ba concentration (10^{-6} mol/kg)		
	Reference $(Ba_{0.95}Sr_{0.05})SO_4$_5 g/kg_90	**Reference $(Ba_{0.83}Sr_{0.17})SO_4$_5 g/kg_90**	**Reference $(Ba_{0.71}Sr_{0.29})SO_4$_5 g/kg_90**
1	25.2	5.46	5.25
3	16.7	6.30	5.80
7	14.0	5.26	5.09
14	14.2	5.18	5.10
21	11.1	3.86	4.09
30	12.9	4.34	4.85
42	10.2	4.17	3.97
56	9.22	3.60	3.63
70	11.6	4.81	4.70
98	11.9	4.46	4.38
133	11.7	4.46	4.63
161	13.8	4.96	5.00
224	12.3	4.52	4.43
294	10.9	3.80	3.41
406	11.2	3.91	4.09
525	11.6	4.46	4.31
664	13.2	6.05	5.57
Equilibrium (GEMS)	6.97	4.19	4.19

Table A13. Sr concentrations of the experiments at 23 °C.

Day	Sr Concentration (10^{-5} mol/kg)		
	$(Ba_{0.95}Sr_{0.05})SO_4$_0.5 g/kg_RT	$(Ba_{0.83}Sr_{0.17})SO_4$_0.5 g/kg_RT	$(Ba_{0.71}Sr_{0.29})SO_4$_0.5 g/kg_RT
1	0.92	15.7	17.5
3	0.81	12.2	29.7
7	0.85	10.6	17.3
14	0.79	10.3	18.9
21	0.77	10.9	17.9
30	0.82	11.2	18.3
42	0.78	11.2	19.6
56	0.90	11.1	23.7
70	0.87	11.1	28.9
98	0.84	13.9	33.2
133	0.84	18.1	37.7
161	0.90	19.8	40.2
224	0.85	22.3	42.3
294	0.86	25.3	44.2
406	1.13	26.6	44.0
525	2.51	26.6	45.1
664	3.16	28.2	49.3
Equilibrium (GEMS)	10.8	37.4	65.2

Table A14. Sr concentrations of reference experiments without Ra at 23 °C.

Day	Sr Concentration (10^{-5} mol/kg)		
	Reference $(Ba_{0.95}Sr_{0.05})SO_4$_0.5 g/kg_RT	Reference $(Ba_{0.83}Sr_{0.17})SO_4$_0.5 g/kg_RT	Reference $(Ba_{0.71}Sr_{0.29})SO_4$_0.5 g/kg_RT
1	0.95	10.7	21.4
3	0.98	10.1	22.0
7	0.12	10.8	22.1
14	0.67	40.6	21.9
21	0.88	12.7	15.9
30		13.4	14.6
42	1.17	13.9	33.6
56	0.77	14.4	32.4
70	0.90	15.3	34.2
98	4.20	16.6	35.0
133	0.51	18.9	56.1
161	0.74	17.9	39.9
224	0.85	19.3	42.3
294	0.75	20.2	43.5
406	1.08	24.4	43.7
525	0.90	21.9	42.7
664	0.88	24.2	44.6
Equilibrium (GEMS)	10.8	37.5	65.4

Table A15. Sr concentration of experiments at 70 °C.

Day	Sr Concentration (10^{-5} mol/kg)		
	$(Ba_{0.95}Sr_{0.05})SO_4$_0.5 g/kg_70	$(Ba_{0.83}Sr_{0.17})SO_4$_0.5 g/kg_70	$(Ba_{0.71}Sr_{0.29})SO_4$_0.5 g/kg_70
1	1.00	11.6	23.7
3	1.10	14.45	23.1
7	2.32	12.1	30.7
14	1.05	15.0	44.3
21	1.09	21.6	47.1
30	1.45	25.8	50.5
42	2.52	27.3	52.7
56	3.73	33.2	54.3
70	3.42	36.6	51.9
98	3.65	34.4	55.1
133	6.22	36.3	68.0
161	4.13	36.8	55.2
224	4.61	39.5	57.6
294	4.49	39.7	55.8
406	4.75	74.0	50.4
525	5.32	42.8	48.5
664	6.21	36.2	50.9
Equilibrium (GEMS)	10.7	37.0	64.0

Table A16. Sr concentration of reference experiments without Ra at 70 °C.

Day	Sr Concentration (10^{-5} mol/kg)		
	Reference $(Ba_{0.95}Sr_{0.05})SO_4$_0.5 g/kg_70	Reference $(Ba_{0.83}Sr_{0.17})SO_4$_0.5 g/kg_70	Reference $(Ba_{0.71}Sr_{0.29})SO_4$_0.5 g/kg_70
1	1.59	11.8	39.4
3	2.27	13.5	34.1
7	1.70	14.5	38.0
14	1.50	16.9	42.0
21	1.72	16.0	47.1
30	1.78	16.3	48.4
42	2.66	16.7	49.6
56	2.04	17.6	51.4
70	2.20	18.4	54.1
98	2.27	20.0	52.4
133	2.36	21.7	59.7
161	2.35	22.9	56.1
224	2.53	22.1	54.8
294	2.41	26.6	19.8
406	2.75	31.4	48.7
525	1.63	28.9	46.0
664	1.77	28.3	56.6
Equilibrium (GEMS)	10.7	37.1	64.4

Table A17. Sr concentration of experiments at 90 °C.

Day	Sr Concentration (10^{-5} mol/kg)		
	$(Ba_{0.95}Sr_{0.05})SO_4$_0.5 g/kg_90	$(Ba_{0.83}Sr_{0.17})SO_4$_0.5 g/kg_90	$(Ba_{0.71}Sr_{0.29})SO_4$_0.5 g/kg_90
1	0.69	43.2	22.6
3	0.99	13.5	28.0
7	1.20	16.2	35.7
14	1.35	21.0	39.8
21	2.00	24.1	42.5
30	2.57	26.4	43.6
42	2.95	28.2	
56	3.19	29.6	52.5
70	3.35	31.1	49.9
98	3.32	31.2	47.9
133	3.53	31.4	47.4
161	3.57	31.1	43.3
224	3.72	32.9	47.5
294	3.74	32.9	47.2
406	3.98	37.0	56.1
525	4.60	33.7	48.7
664	5.40	37.9	65.3
Equilibrium (GEMS)	10.7	36.7	62.7

Table A18. Sr concentration of reference experiments without Ra at 90 °C.

Day	Sr Concentration (10^{-5} mol/kg)		
	Reference $(Ba_{0.95}Sr_{0.05})SO_4$_0.5 g/kg_90	Reference $(Ba_{0.83}Sr_{0.17})SO_4$_0.5 g/kg_90	Reference $(Ba_{0.71}Sr_{0.29})SO_4$_0.5 g/kg_90
1	1.40	11.9	26.0
3	1.27	13.9	37.6
7	1.34	16.8	35.2
14	1.35	18.9	38.7
21	1.43	20.4	41.7
30	1.25	21.0	41.8
42	1.45	22.1	43.4
56	1.48	23.4	
70	1.40	24.5	47.4
98	1.60	13.3	48.6
133	1.54	26.0	46.1
161	1.75	25.6	45.6
224	1.66	26.8	48.4
294	1.91	27.0	48.7
406	1.90	31.1	50.6
525	1.63	28.9	46.0
664	1.77	28.3	56.6
Equilibrium (GEMS)	10.7	36.7	63.3

Table A19. Sr concentration of experiments at 90 °C and S/L = 5 g/kg.

Day	Sr Concentration (10^{-5} mol/kg)		
	$(Ba_{0.95}Sr_{0.05})SO_4$_5 g/kg_90	$(Ba_{0.83}Sr_{0.17})SO_4$_5 g/kg_90	$(Ba_{0.71}Sr_{0.29})SO_4$_5 g/kg_90
1	8.81	37.3	42.1
3	10.6	45.0	51.7
7	12.7	48.2	55.2
14	16.0	51.0	60.7
21	17.5	52.6	59.9
30	18.5	54.9	61.5
42	20.3	64.6	61.5
56	21.3	77.7	64.1
70	21.9	56.9	68.3
98	22.2		66.6
133	23.0	58.1	68.0
161	23.3	59.0	72.4
224	23.7	60.5	71.4
294	23.3	60.1	68.2
406	28.4	74.9	85.0
525	35.7	74.7	77.3
664	36.2	70.9	77.4
Equilibrium (GEMS)	63.1	113	113

Table A20. Sr concentration of reference experiments without Ra at 90 °C and S/L = 5 g/kg.

Day	Sr Concentration (10^{-5} mol/kg)		
	Reference $(Ba_{0.95}Sr_{0.05})SO_4$_5 g/kg_90	Reference $(Ba_{0.83}Sr_{0.17})SO_4$_5 g/kg_90	Reference $(Ba_{0.71}Sr_{0.29})SO_4$_5 g/kg_90
1	9.60	38.9	40.1
3	11.3	40.6	46.3
7	12.8	47.1	50.8
14	14.0	44.9	52.0
21	14.7	51.2	55.3
30	16.1	53.5	58.2
42	16.1	55.0	55.7
56	16.6	50.9	57.5
70	17.5	55.1	59.2
98	42.7	57.0	59.3
133	18.0	60.4	60.1
161	17.9	56.8	60.0
224	18.3	58.7	60.0
294	18.4	50.7	60.8
406	20.8	66.1	71.7
525	18.7	65.9	85.9
664	18.2	61.3	71.1
Equilibrium (GEMS)	66.8	114	114

Table A21. Temporal evolution of the solid composition analyzed by EDX of $(Ba_{0.95}Sr_{0.05})SO_4$_0.5 g/kg_RT. Superscript numbers indicate spot measurements in Figure 5.

Day	Particle	X_{SrSO4} (%)	X_{RaSO4} (%)	X_{BaSO4} (%)
$(Ba_{0.95}Sr_{0.05})SO_4$_0.5 g/kg_RT				
1	P1	4.6	<0.5	95.1
	P2	4.5	0.8	94.7
	P3	4.8	<0.5	95.0
	P4	3.5	0.6	95.9
	P5	9.8	n.d.	90.2
Average EDX		**5.4**		**94.2**
Average mass balance		**5.6**	**0.04**	**95.4**
42	P1	7.3	<0.5	92.5
	P1	3.9	<0.5	95.8
	P2	3.9	<0.5	95.9
	P3	3.5	0.5	96.0
	P3	8.2	0.5	91.3
	P4	6.0	<0.5	93.8
	P5	2.9	<0.5	96.9
Average EDX		**5.1**		**94.6**
Average mass balance		**4.7**	**0.03**	**95.3**
98	P1	3.7	n.d.	96.3
	P1	3.2	n.d.	96.8
	P2	10.1	<0.5	89.8
	P2	10.3	<0.5	89.4
	P3	5.0	n.d.	95.0
	P4	3.3	<0.5	96.5
	P5	4.7	<0.5	95.0
Average EDX		**5.8**		**94.1**
Average mass balance		**4.7**	**0.03**	**95.3**
664	P1	4.1	<0.5	95.7
	P1	4.2	<0.5	95.7
	P2	3.6	<0.5	96.2
	P2	4.4	<0.5	95.2
	P3	5.7	<0.5	93.9
	P3	7.0	<0.5	92.8
	P4	3.8	<0.5	95.9
	P4	4.1	<0.5	95.6
	P5	5.0	<0.5	94.7
	P5	4.5	0.7	94.9
	P5	2.8	1.2	95.8
	P6	5.5	<0.5	93.8
	P6	5.8	<0.5	93.9
	P7	3.4	<0.5	96.4
	P7	4.1	<0.5	95.7
	P7	2.0	0.5	97.5
	P8	0.4	0.7	98.9
	P8	1.3	1.2	97.5
	P8	1.2	2.7	95.3
	P9	1.3	0.8	97.9
	P9	6.6	0.7	93.4
Average EDX		**3.8**		**95.6**
Average mass balance		**3.6**	**0.03**	**96.1**
Calculated equilibrium		**0.3**	**0.02**	**99.7**

n.d. not detected.

Table A22. Temporal evolution of the solid composition analyzed by EDX of $(Ba_{0.71}Sr_{0.29})SO_4$_0.5 g/kg_RT. Superscript numbers indicate spot measurements in Figure 5.

Day	Particle	X_{SrSO4}	X_{RaSO4}	X_{BaSO4}
		(%)	(%)	(%)
	$(Ba_{0.71}Sr_{0.29})SO_4$_0.5 g/kg_RT			
1	P1	27.4	n.d.	72.6
	P1	5.8	<0.5	93.8
	P1	20.8	<0.5	78.9
	P2	9.2	<0.5	90.7
	P2	8.1	0.5	91.5
	P3	30.5	<0.5	69.3
	P3	27.4	n.d.	72.6
	P3	22.3	<0.5	77.4
	P4	9.0	<0.5	90.5
	P4	15.8	1.59	82.6
	P5	23.9	<0.5	75.8
	P6	4.3	<0.5	95.4
Average EDX		**17.0**		**82.6**
Average mass balance		**23.2**	**0.1**	**76.6**
42	P1	6.5	1.1	92.8
	P1	21.6	<0.5	78.0
	P2	8.4	<0.5	91.1
	P3	7.3	2.8	89.9
	P3	5.4	2.4	92.2
	P4	11.2	1.1	87.8
	P4	27.9	<0.5	71.7
	P5	23.1	<0.5	76.7
	P5	9.1	0.6	90.3
Average EDX		**13.4**		**85.6**
Average mass balance		**22.3**	**0.3**	**77.4**
98	P1	7.9	0.9	91.2
	P2	22.7	<0.5	76.9
	P2	17.6	<0.5	82.2
	P2	6.9	<0.5	92.8
	P3	11.8	<0.5	87.8
	P3	15.4	<0.5	84.5
	P4	17.3	0.7	82.0
	P5	12.9	1.0	86.1
	P6	11.9	0.9	87.3
	P6	24.3	<0.5	75.3
	P6	14.8	<0.5	84.8
Average EDX		**14.1**		**85.4**
Average mass balance		**16.9**	**0.3**	**82.8**

Table A22. *Cont.*

Day	Particle	X_{SrSO4} (%)	X_{RaSO4} (%)	X_{BaSO4} (%)
664	P1	9.9	0.6	89.6
	P1	9.8	0.5	89.7
	P2	11.6	0.5	87.9
	P2	10.5	<0.5	89.3
	P3	7.8	<0.5	91.9
	P4	7.2	<0.5	92.5
	P4	8.1	0.5	91.4
	P4	8.9	n.d.	91.1
	P5	21.4	<0.5	78.4
	P5	5.0	<0.5	94.6
	P5	9.0	<0.5	90.9
	P5	11.7	0.7	87.6
	P6	9.0	<0.5	90.7
	P6	5.2	<0.5	94.5
	P6	8.4	<0.5	91.3
	P7	5.3	0.5	94.2
	P7	10.3	<0.5	89.4
	P7	4.7	<0.5	95.0
	P8	8.2	<0.5	91.5
	P8	10.0	1.4	88.6
	P8	7.4	<0.5	92.2
	P9	21.3	<0.5	78.3
	P9	10.0	0.5	89.5
	P10	9.6	0.8	89.6
	P10	17.4	<0.5	82.3
Average EDX		**9.9**		**89.7**
Average mass balance		**9.5**	**0.4**	**90.2**
Calculated equilibrium		**0.6**	**0.3**	**99.1**

n.d. not detected.

Table A23. Temporal evolution of the solid composition analyzed by EDX of $(Ba_{0.95}Sr_{0.05})SO_4$_5 g/kg_90. Superscript numbers indicate spot measurements in Figure 5.

Day	Particle	X_{SrSO4} (%)	X_{RaSO4} (%)	X_{BaSO4} (%)
	$(Ba_{0.95}Sr_{0.05})SO_4$_5 g/kg_90			
1	P1	10.3	<0.5	89.5
	P1	12.8	n.d	87.2
	P1	13.6	<0.5	86.5
	P2	10.1	n.d	89.9
	P2	3.9	1.7	94.4
	P3	4.0	<0.5	95.6
	P4	4.9	<0.5	94.6
Average EDX		**8.5**		**91.1**
Average mass balance		**4.6**	**0.03**	**95.4**
42	P1	4.1	0.5	95.4
	P1	1.5	0.7	97.1
	P2	2.0	<0.5	97.8
	P3	4.0	<0.5	95.9
	P4	1.0	<0.5	98.8
Average EDX		**2.5**		**97.0**
Average mass balance		**4.1**	**0.03**	**95.9**

Table A23. *Cont.*

Day	Particle	X_{SrSO4} (%)	X_{RaSO4} (%)	X_{BaSO4} (%)
98	P1	2.6	<0.5	97.2
	P2	1.6	0.98	97.4
	P3	1.5	<0.5	98.2
	P4	7.0	<0.5	91.8
	P5	0.8	<0.5	99.0
	P6	4.4	<0.5	95.5
Average EDX		**3.0**		**96.5**
Average mass balance		**4.0**	**0.03**	**96.0**
664	P1	3.4	<0.5	96.3
	P2	6.3	n.d	93.7
	P2	6.0	<0.5	93.8
	P3	3.1	<0.5	96.5
	P3	2.3	0.6	97.1
	P4	4.4	<0.5	95.2
	P4	5.0	<0.5	94.9
	P5	1.6	<0.5	98.0
	P5	2.7	<0.5	97.2
	P6	5.8	<0.5	94.0
	P6	3.8	<0.5	95.9
	P7	2.2	0.5	97.3
	P8	4.8	<0.5	95.0
	P9	3.2	0.6	96.2
Average EDX		**3.9**		**95.8**
Average mass balance		**3.4**	**0.03**	**96.6**
Calculated equilibrium		**2.2**	**0.02**	**97.8**

References

1. Rutherford, P.M.; Dudas, M.J.; Arocena, J.M. Heterogeneous distribution of radionuclides, barium and strontium in phosphogypsum by-product. *Sci. Total Environ.* **1996**, *180*, 201–209. [CrossRef]
2. Fisher, R.S. Geologic and Geochemical Controls on Naturally Occurring Radioactive Materials (NORM) in Produced Water from Oil, Gas, and Geothermal Operations. *Environ. Geosci.* **1998**, *5*, 139–150. [CrossRef]
3. Burnett, W.C.; Elzerman, A.W. Nuclide migration and the environmental radiochemistry of Florida phosphogypsum. *J. Environ. Radioact.* **2001**, *54*, 27–51. [CrossRef]
4. Martin, A.J.; Crusius, J.; McNee, J.J.; Yanful, E.K. The mobility of radium-226 and trace metals in pre-oxidized subaqueous uranium mill tailings. *Appl. Geochem.* **2003**, *18*, 1095–1110. [CrossRef]
5. Liu, D.J.; Hendry, M.J. Controls on ^{226}Ra during raffinate neutralization at the Key Lake uranium mill, Saskatchewan, Canada. *Appl. Geochem.* **2011**, *26*, 2113–2120. [CrossRef]
6. Zhang, T.; Gregory, K.; Hammack, R.W.; Vidic, R.D. Co-precipitation of Radium with Barium and Strontium Sulfate and Its Impact on the Fate of Radium during Treatment of Produced Water from Unconventional Gas Extraction. *Environ. Sci. Technol.* **2014**, *48*, 4596–4603. [CrossRef]
7. Norrby, S.; Andersson, J.; Dverstorp, B.; Kautsky, F.; Lilja, C.; Sjöblom, R.; Sundström, B.; Toverud, Ö.; Wingefors, S. *SKI SITE-94 Saekerhetsanalys foer Djupfoervar iett Kristallint berg*; Svensk Kärnbränslehantering AB (SKB): Stockholm, Sweden, 1997.
8. Grandia, F.; Merino, J.; Bruno, J. *Assessment of the Radium-Barium Co-Precipitation and Its Potential Influence on the Solubility of Ra in the Near-Field*; SKB Technical Report TR-08-07; SKB: Stockholm, Sweden, 2008.
9. NAGRA. Technischer Bericht NTW 14-03. In *Charakteristische Dosisintervalle und Unterlagen zur Bewertung der Barrierensysteme*; NAGRA: Wettingen, Switzerland, 2014.
10. Curti, E.; Xto, J.; Borca, C.N.; Henzler, K.; Huthwelker, T.; Prasianakis, N.I. Modelling Ra-bearing baryte nucleation/precipitation kinetics at the pore scale: Application to radioactive waste disposal. *Eur. J. Mineral.* **2019**, 247–262. [CrossRef]

11. Zhu, C. Coprecipitation in the barite isostructural family: 1. binary mixing properties. *Geochim. Cosmochim. Acta* **2004**, *68*, 3327–3337. [CrossRef]
12. Rosenberg, Y.O.; Metz, V.; Ganor, J. Co-precipitation of radium in high ionic strength systems: 1. Thermodynamic properties of the Na-Ra-Cl-SO_4-H_2O system—Estimating Pitzer parameters for $RaCl_2$. *Geochim. Cosmochim. Acta* **2011**, *75*, 5389–5402. [CrossRef]
13. Rosenberg, Y.O.; Sadeh, Y.; Metz, V.; Pina, C.M.; Ganor, J. Nucleation and growth kinetics of $Ra_xBa_{1-x}SO_4$ solid solution in NaCl aqueous solutions. *Geochim. Cosmochim. Acta* **2014**, *125*, 290–307. [CrossRef]
14. Curti, E.; Fujiwara, K.; Iijima, K.; Tits, J.; Cuesta, C.; Kitamura, A.; Glaus, M.A.; Müller, W. Radium uptake during barite recrystallization at 23 ± 2 °C as a function of solution composition: An experimental ^{133}Ba and ^{226}Ra tracer study. *Geochim. Cosmochim. Acta* **2010**, *74*, 3553–3570. [CrossRef]
15. Klinkenberg, M.; Brandt, F.; Breuer, U.; Bosbach, D. Uptake of Ra during the recrystallization of barite: A microscopic and time of flight-secondary ion mass spectrometry study. *Environ. Sci. Technol.* **2014**, *48*, 6620–6627. [CrossRef] [PubMed]
16. Torapava, N.; Ramebäck, H.; Curti, E.; Lagerkvist, P.; Ekberg, C. Recrystallization of ^{223}Ra with barium sulfate. *J. Radioanal. Nucl. Chem.* **2014**, *301*, 545–553. [CrossRef]
17. Brandt, F.; Curti, E.; Klinkenberg, M.; Rozov, K.; Bosbach, D. Replacement of barite by a (Ba,Ra)SO_4 solid solution at close-to-equilibrium conditions: A combined experimental and theoretical study. *Geochim. Cosmochim. Acta* **2015**. [CrossRef]
18. Prieto, M.; Heberling, F.; Rodríguez-Galán, R.M.; Brandt, F. Crystallization behavior of solid solutions from aqueous solutions: An environmental perspective. *Prog. Cryst. Growth Charact. Mater.* **2016**, *62*, 29–68. [CrossRef]
19. Heberling, F.; Metz, V.; Böttle, M.; Curti, E.; Geckeis, H. Barite recrystallization in the presence of ^{226}Ra and ^{133}Ba. *Geochim. Cosmochim. Acta* **2018**. [CrossRef]
20. Rollog, M.; Cook, N.J.; Guagliardo, P.; Ehrig, K.J.; Kilburn, M. Radionuclide-bearing minerals in Olympic Dam copper concentrates. *Hydrometallurgy* **2019**, *190*, 105153. [CrossRef]
21. Schmandt, D.S.; Cook, N.J.; Ehrig, K.; Gilbert, S.; Wade, B.P.; Rollog, M.; Ciobanu, C.L.; Kamenetsky, V.S. Uptake of trace elements by baryte during copper ore processing: A case study from Olympic Dam, South Australia. *Miner. Eng.* **2019**, *135*, 83–94. [CrossRef]
22. Vinograd, V.L.; Brandt, F.; Rozov, K.; Klinkenberg, M.; Refson, K.; Winkler, B.; Bosbach, D. Solid-aqueous equilibrium in the $BaSO_4$-$RaSO_4$-H_2O system: First-principles calculations and a thermodynamic assessment. *Geochim. Cosmochim. Acta* **2013**, *122*, 398–417. [CrossRef]
23. Vinograd, V.L.; Kulik, D.A.; Brandt, F.; Klinkenberg, M.; Weber, J.; Winkler, B.; Bosbach, D. Thermodynamics of the solid solution—Aqueous solution system (Ba,Sr,Ra)SO_4 + H_2O: I. The effect of strontium content on radium uptake by barite. *Appl. Geochem.* **2018**, *89*, 59–74. [CrossRef]
24. Vinograd, V.L.; Kulik, D.A.; Brandt, F.; Klinkenberg, M.; Weber, J.; Winkler, B.; Bosbach, D. Thermodynamics of the solid solution—Aqueous solution system (Ba,Sr,Ra)SO_4 + H_2O: II. Radium retention in barite-type minerals at elevated temperatures. *Appl. Geochem.* **2018**, *93*, 190–208. [CrossRef]
25. Klinkenberg, M.; Weber, J.; Barthel, J.; Vinograd, V.; Poonoosamy, J.; Kruth, M.; Bosbach, D.; Brandt, F. The solid solution–aqueous solution system (Sr,Ba,Ra)SO_4 + H_2O: A combined experimental and theoretical study of phase equilibria at Sr-rich compositions. *Chem. Geol.* **2018**, *497*, 1–17. [CrossRef]
26. Patel, A.R.; Bhat, H.L. Growth of strontium sulphate single crystals by chemically reacted flux and their dislocaton configuration. *J. Cryst. Growth* **1971**, *8*, 153–156. [CrossRef]
27. Patel, A.R.; Koshy, J. Growth of barium sulphate single crystals by chemically reacted flux. *J. Cryst. Growth* **1968**, *2*, 128–130. [CrossRef]
28. Kulik, D.A.; Wagner, T.; Dmytrieva, S.V.; Kosakowski, G.; Hingerl, F.F.; Chudnenko, K.V.; Berner, U.R. GEM-Selektor geochemical modeling package: Revised algorithm and GEMS3K numerical kernel for coupled simulation codes. *Comput. Geosci.* **2013**, *17*, 1–24. [CrossRef]
29. Helgeson, H.C.; Kirkham, D.H.; Flowers, G.C. Theoretical prediction of the thermodynamic behavior of aqueous electrolytes by high pressures and temperatures; IV, Calculation of activity coefficients, osmotic coefficients, and apparent molal and standard and relative partial molal properties to 600 d. *Am. J. Sci.* **1981**, *281*, 1249–1516. [CrossRef]
30. Thoenen, T.; Hummel, W.; Berner, U.; Curti, E. *The PSI/Nagra Chemical Thermodynamic Database 12/07*; Nuclear Energy and Safety Research Department Laboratory for Waste Management (LES): Villigen, Switzerland, 2014.

31. Weber, J.; Barthel, J.; Klinkenberg, M.; Bosbach, D.; Kruth, M.; Brandt, F. Retention of ^{226}Ra by barite: The role of internal porosity. *Chem. Geol.* **2017**, *466*, 722–732. [CrossRef]
32. Brandt, F.; Klinkenberg, M.; Poonoosamy, J.; Weber, J.; Bosbach, D. The Effect of Ionic Strength and Sr_{aq} upon the Uptake of Ra during the Recrystallization of Barite. *Minerals* **2018**, *8*, 502. [CrossRef]
33. Poonoosamy, J.; Klinkenberg, M.; Deissmann, G.; Brandt, F.; Bosbach, D.; Mäder, U.; Kosakowski, G. Effects of solution supersaturation on barite precipitation in porous media and consequences on permeability: Experiments and modelling. *Geochim. Cosmochim. Acta* **2020**, *270*, 43–60. [CrossRef]